Simultaneous control rod 3D displacement and 3D flow measurements via time resolved 3D3C PTV with one camera only

Vincent Fichet, Mouad Daoudi, Laurent Zimmer

SIMULTANEOUS CONTROL ROD 3D DISPLACEMENT AND 3D FLOW MEASUREMENTS VIA TIME RESOLVED 3D3C PTV WITH ONE CAMERA ONLY

Vincent FICHET
Technical Center Framatome, 71200 Le Creusot, France
Mouad DAOUDI
CNRS PC2A Laboratory UMR 8522, 59000 Lille, France
Laurent ZIMMER
Université Paris-Saclay, CNRS, CentraleSupélec, Laboratoire EM2C, 91190, Gif-sur-Yvette, France.

ABSTRACT

In the framework of Flow-Induced Vibration (FIV), the measuring capability of a time-resolved 3D-3C Particle Tracking Velocimetry (PTV) with one camera only is addressed in this paper. The study deals with a representative turbulent flow ($Re = 3.10^4$) around guide plates and simulated control rods as parts of a nuclear CRGA (Control Rod Guide Assembly). Based on image defocus, this 3D3C PTV transforms the scattered light of laser-illuminated seeding particles into circular patterns on the defocused images. A patented annular pupil device is used in this scope. These particle patterns are detected and tracked over time by PTV in order to provide instantaneous 3D velocity fields. 3D3C PTV velocities are validated by comparison with LDV data for both spatial (mean and standard deviation of velocity) and spectral (PSD) domains to confirm the accurate capture of the flow dynamics. The measures are found to be consistent in both shape and amplitude. The 3D3C PTV measurements are even more refined than LDV near the rods for the main axial flow. An easy, non-intrusive in-situ calibration based on a laser sheet sweep along the camera's in-depth direction completes the technique. The time required to post-process 20 000 images (time points) is less than 24 h on an HP Z820 workstation with 24 cores, and more than 1000 particles can be tracked per image over time to create trajectories.

Simultaneously, the 3D displacement of moving rods is recorded on these images (one camera only). Tracer particles are indeed fixed on the moving rods to track the rod FIV. Two moving rods are scrutinized in the upstream vicinity of a guide plate: one "free rod" is submitted to flexion with pinned-pinned boundary conditions, and another is held by strings in the highest cross-flow velocity region. With the same set of defocused images, the technique describes then both the excitation (flow) and the rod response (displacement) at the same time, leading to the whole Fluid-Structure Interaction (FSI) or the structure transfer function (response/excitation) with one camera only. The missing step that remains will be to reconstruct instantaneous pressure fields from 3D3C particle trajectories to reach the fluid loads applied to the structure (here rods). Previous works were already undertaken at Technical Center Framatome in 2014 to meet this objective.

1. INTRODUCTION

In Pressurised Water Reactors (PWR), the nuclear reactions are controlled by Rod Cluster Control Assemblies (RRCA). This RCCA is composed of control rods, imprinted with neutron absorbing material and inserted or withdrawn into the Fuel Assemblies (FA) by moving vertically a drive shaft connected to a spider to which control rods are fixed at their upper end. The control rods are about 4 *m* long for 10 *mm* diameter making them very flexible (ratio "length/diameter" around 400). They need then to be guided before entering the FA located further down. Two guiding sections, separated by a support plate, are commonly used. Discontinuous guidance is ensured in the upper section via a set of guide plates regularly spaced from each other (see Figure 1).

In the lower section, control rods are first guided via another set of guide plates and then pass through continuous guidance (opened tubes) before entering the FA. The upwards coolant flow coming from each FA passes through the Upper Core Plate (UCP) before entering the continuous guidance and the sets of guide plates. A mainly axial flow then takes place along the RCCA height. However, cross-flows are generated around the guide plates due to their star-shaped cross-sections, adding excitation to the control rods subject to FIV. These vibrations could cause fatigue and fretting wear of the materials and lead to maintenance operations. Consequently, a dedicated understanding of this FIV based on reliable experi-

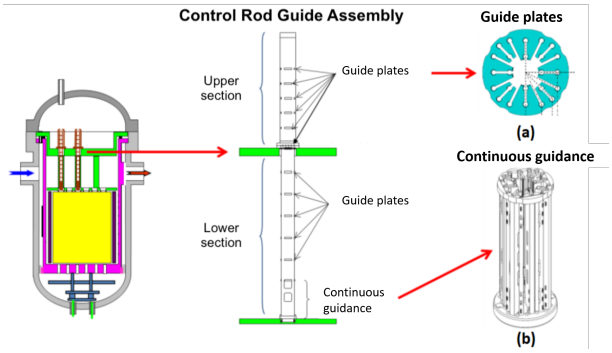

Figure 1. CRGA location in a nuclear reactor, ***(a)*** *Guide plates,* ***(b)*** *Continuous guidance, adapted from Fichet et al (2018)*

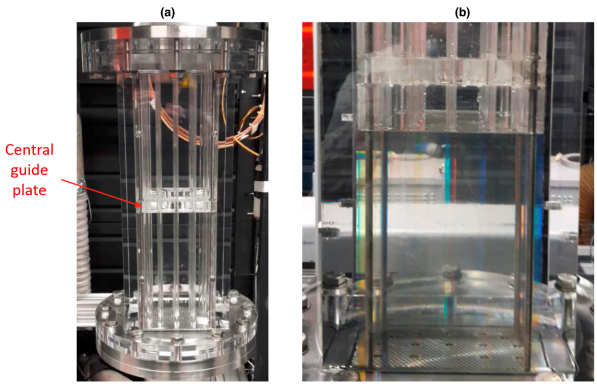

Figure 2. Transparent guide plates mock-up: ***(a)*** *Test section,* ***(b)*** *Index matching during immersion of the rods below the central guide plate, adapted from Fichet et al (2018))*

mental data is required. Over the years, several attempts have been made to measure the control rod vibration. Shono et al. (1985) used the noise analysis technique with the neutron flux (reactivity signal from the primary flow rate), load weight of control rods and an acoustic signal of the control rod driving mechanism to estimate the control rods' vibration mode and the correspondent driving forces. The same neutron noise approach was validated by Ansari et al (2008) by deploying a reactor internals vibration monitoring system. Later on, Kim et al (2001) used a non-contact laser vibrometer and a digital oscilloscope to measure real-time rod vibration and concluded that the turbulence excitation is the most probable variation mechanism of RCCA. Moussou et al (2019) reach the same conclusions when analyzing the FIV of the control rod in a full scale 1300 MWe CRGA mock-up. De Pauw et al (2013) investigated six vibration measuring techniques to tackle the FIV on a fuel pin mock-up. These techniques included Laser Doppler Velocimetry (LDV), a grid method (GRID), fibre Bragg grating sensors (FBGs), electrical strain gages and two types of accelerometers. The study concluded that LDV and MEMs-type accelerometer techniques offer superior performance. For space constraints, the authors believe that the FBGs technique is the most suitable one when dealing with vibration monitoring in nuclear reactor core mock-ups. LDV was also investigated by Shengjie et al (2015) and was found to provide more accurate results compared to traditional accelerometer methods. Unfortunately, all the studies mentioned before focus only on measuring the rod's response and do not provide any extensive data on the flow excitation around those vibrating structures.

One of the first attempts to provide experimental data for both the mechanical response and the flow field was proposed by Cioncolini et al (2018). The authors conducted experiments on a considerably simplified geometry in which a single clamped-free cantilevered cylindrical rod confined in a tube and subject to axial flow directed from the rod free-end towards the clamped-end was used. The study used a non-contact optical technique to measure the 3D rod displacement along with 2D Particle Imaging Velocimetry (PIV) to measure the velocity field, making the experimental setup quite delicate to handle since it uses two different cameras. To the best of the author's knowledge, 3D flow measurements simultaneously with rod 3D displacement have not been yet dealt with. The present investigation was therefore conducted to match such requirements and to consolidate the FIV/FSI Computational Fluid Dynamics (CFD) models with a relatively simple but representative setup.

In this study, 3D3C PTV is conducted on control rods placed in a full-scale guide plate mock-up (see Figure 2). The 3D3C PTV principle is reminded in section 2.2. The velocities obtained are found to be more accurate than former results (see Fichet et al (2018)), especially near the rod submitted to FIV and are confronted to Laser Doppler Velocimetry (LDV) in section 3.1. Finally, an innovative tracking technique (see section 2.3) is presented to capture the 3D displacement of a moving rod simultaneously with the 3D instantaneous velocity field, using the same set of defocused images. The associated results are presented in section 3.2.

2. EXPERIMENTAL SETUP AND POST-PROCESSING

2.1. Mock-up and instrumentation

The current turbulent flow is to be linked to the one produced inside a CRGA of a nuclear reactor.

However, non-intrusive measurements, such as 3D3C PTV in a fully transparent mock-up to capture the velocity field finely around the obstacle, can not be undertaken in real-operating conditions due to the rod material, the fluid pressure and temperature. Therefore, the study is limited to the same mean flow rate Q (similitude inflow velocity) in a representative geometry (star-shape of the guide plate cross-section) but at ambient pressure P and temperature T conditions as mentioned in Table 1. The mock-up consists of two guide plates distant by 293 *mm* from each other, along with control rods (up to 24 in Figure 2) at full scale. The simulated guide plates exhibit a square shape (173 *mm* side) to reduce the optical distortions on the test section surface, making them slightly different from the real ones in nuclear reactors. The studied guide plate is the one located in the middle (height) of the test section. It is positioned and fixed in the test section via rigid steel threaded rods in its four corners. Both control rods and guide plates are made of Plexiglass to enable non-intrusive laser measurements. In addition, an index-matching technique used at Technical Center Framatome for more than ten years is deployed. The concentration of a dedicated solution of sodium iodide, used as the driven fluid, is fine-tuned to match the refracting index of Plexiglass parts ($n \approx 1.49$). When index matching is reached, the solid parts almost disappear and enable an optimal visualization of the particles even behind the obstacles to get a full 3D view of the velocities surrounding the rod. Considering the fluid properties and geometric scales (see Table 1), the turbulent ascending flow is established with a Reynolds number of 3.10^4.

Quantity	Value
$Q\ (l/s)$	19.17
$P\ (bar)$	1
$T\ (C)$	25
$\rho\ (kg/m^3)$	1798
$\nu\ (m^2/s)$	$1.76.10^{-6}$
Re_H	3.10^4
$D_H\ (mm)$	78.1
$V_{\text{inlet}}\ (m/s)$	0.68

Table 1. Guide plates mock-up operating conditions and fluid properties

First, PIV is performed in a vertical symmetry plane crossing the guide plates to identify the flow topology and regions with velocity gradients (see Figure 3). Even with an imperfect upstream flow (i.e. not a flat axial velocity profile), the flow formed downstream the star-shaped diaphragm of the guide plate appears quite symmetrical. A large central jet is generated with a high velocity, maintained up to

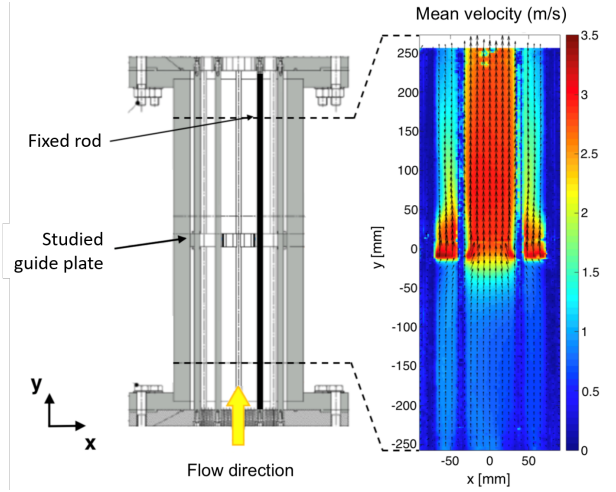

Figure 3. Location of the fixed rod (in black) in the Two-guide plates mock-up and mean velocity field (over 500 instants) in the median plane resulting from a PIV measurement

the next guide plate located downstream. At the periphery, jets are also produced downstream of the peripheral slots between the rod locations. These peripheral jets are quickly decreasing in velocity along the elevation. The peripheral jets indeed feed the main central jet with momentum, which explains the former observations. Recycling zones are also produced around the central jet and induce velocity fluctuations, especially when interacting with peripheral jets.

Three setup configurations are then realized with 3D3C PTV around rods but either upstream or downstream of the central guide plate. In the first one, named **Fixed rod**, a control rod with pinned-pinned boundary conditions passes through an undamaged central guide plate as indicated in black in Figure 3. The second configuration named **Free rod** is similar to the first one except that the central guide plate presents an enlarged gap to let the rod free oscillate towards the guide plate centre. The third configuration is called **Instrumented rod** which is the red portion in Figure 4. The instrumented rod is attached to upper and lower support rods (indicated in blue) using strings. This particular configuration focuses on the upstream vicinity of the central guide plate, the region with the highest cross-flow velocities in order to observe the rod response to this transverse excitation. This latter case best demonstrates the potential of the tracking method introduced in section 2.3. For the fixed rod configuration, 3D3C measurements were made downstream of the central guide plate, whereas the upstream section was investigated for free and instrumented rod configurations.

Defocused images for 3D3C PTV are acquired us-

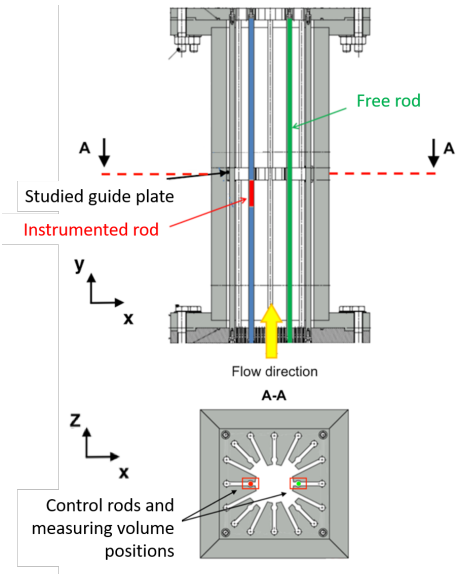

Figure 4. Location of the free rod (in green) and the instrumented rod (in red)

ing a Phantom V611 high-speed camera (up to 6 kHz at full 1280×800 resolution) and a Nikon Nikkor AF-DC 105 mm lens opened at F/2 and the patented annular pupil device. An additional wavelength filter at 570 nm eliminates noise reflections and captures only the light emitted by fluorescent (fluid tracer) seeding particles of an average diameter of 30 μm. On the one hand, a YLF Litron dual cavity laser (up to 6 kHz) with a wavelength of 527 nm and energy 8.5 mJ per pulse at 1 kHz illuminates a fluid volume of $50 \times 40 \times 20\ mm^3$ for 3D3C measurements. On the other hand, LDV measurements, used for validation purposes, are performed using a DANTEC FlowExplorer Laser with a wavelength of 532 nm and maximum output power of 300 mW.

2.2. 3D3C PTV technique

By definition, the 3D3C PTV technique used in this study is based on 3D Lagrangian tracking methods. The method was first developed by Baudoin (2015) during his PhD thesis in collaboration with the EM2C laboratory (CNRS). The technique performance was gradually improved at Technical Center Framatome since then, multiplying by a factor of 100 the number of particles tracked over time (at least three instants) per image. The technique is based on the defocusing principle introduced by Damaschke et al (2005) with which the apparent size of a seed particle on the defocused image is a function of its position in depth (distance to the lens) and the optical mounting characteristics only. Under the assumption of the thin lens and considering seed particles as punctual points (when focusing), if Z_1, f and d_a are the "object" (particle) distance (equal to the image particle distance from the lens plane), the image focal distance and the annular pupil diameter respectively, then the apparent size of that particle on the CCD camera sensor plane d_i is given by Damaschke et al (2005) as expressed in Figure 5.

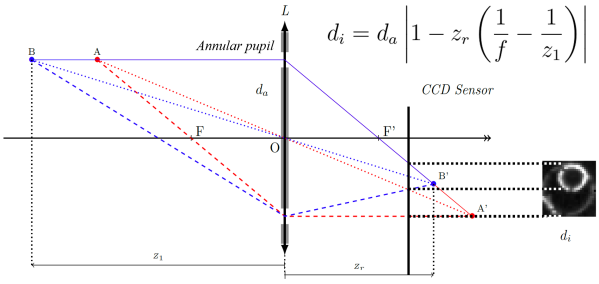

Figure 5. Defocusing principle, adapted from Damaschke et al (2005), Baudoin (2015) and Fichet et al (2018) and the apparent size conversion law, adapted from Damaschke et al (2005)

In the present example (see figure 5), two seeding particles are located at two different distances from the lens (or camera) and placed one behind the other on an axis parallel to the optical axis (see Figure 5). The image obtained on the CCD sensor, when defocusing, show two patterns of different sizes. This "apparent" size of the particles in the defocused image is linked to their position in depth in addition to their locations in the image plane (left/right, up/down). The optical setup is equipped with the patented annular pupil device that generates a circular pattern instead of an entire disc for each particle image. This leads to a much higher particle overlap rate and a better precision in particle positioning.

A typical instantaneous image is displayed in figure 6. One can see the different sizes of the particles, due to their positions in the perpendicular direction with respect to the camera. The rod is in the central part of the picture and therefore presents a lower density of particles with respect to the neighboring zones. Obviously, real optics could not be considered thin lenses. In-situ calibration is then needed to determine the law that links the particle position in-depth to its apparent size on the defocused image. This calibration is easy with one camera. A simple sweep of the laser sheet over the measuring volume along the depth is required. For the present study, the calibration law (apparent particle size into real position in depth) is done by acquiring ten sets of hundreds of frames every 2 mm in depth. Given the number of acquired particles per image and the number of images, one can reach statistical convergence to determine the mean and standard deviation

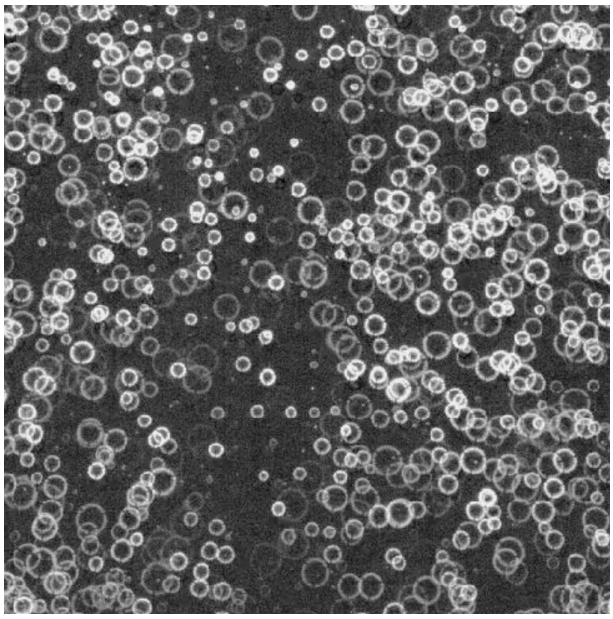

Figure 6. Typical instantaneous image obtained during the experiments

(over the image) of apparent size as a function of the particle position in depth. It has been demonstrated that this calibration behaves as a 3^{rd} order polynomial function (see Fichet et al (2018)). In-plane calibration is based on the rod diameter and the apparent size in the nearest laser plane. 3D3C measurements rely then on image post-processing split in two steps. The first one consists of detecting all particle positions in each frame. Pattern recognition algorithm using cross-correlation with circular pattern canvas (of various sizes) is used and gives the particle positions at a sub-pixel level. The second one is an association algorithm with which each particle is tracked in time to reconstruct its trajectory (from the positions detected) over the time sequence. To support the association process, a PIV-based predictor is calculated for each frame to locate the next particle position in time. Tests are performed to confirm the existence of that particle or not at the next instant. A multi-frame algorithm is used to complete the association process feeding then a 3D predictor with the confirmed associations. Particle trajectories are then reconstructed over time. The verification tests include features that deal with nested particle detection and ghost particles. The last version of those 3D3C PTV algorithms reaches a 0.001 particle per pixel (ppp) resolution. The reconstructed velocity is obtained with a 0.05 px uncertainty in the three directions. For further details about the 3D3C PTV post-processing algorithms, the reader could refer to Baudoin (2015) and Fichet et al (2018).

2.3. Tracking method

As introduced before, the rod's 3D displacement is obtained by tracking fixed seed particles at its surface. In fact, those seed particles appear in the 3D3C recorded frames with an apparent size just like any other seed particle in the measurement volume. However, their motion remains in the camera's field of view along with all the acquisition. Once the fixed particles are identified on the image, dedicated post-processing could be applied based on 3D3C PTV algorithms or finer tracking methods like the Optical Flow (OF). An enhanced version of the 3D3C PTV detection algorithm is used only in the restricted area of the image in which the "rod" particle is moving to gain computational time. Local cross-correlation of the "rod" particle image is then used to track its motion finely even if some filters (criteria) are applied to eliminate inappropriate candidates (in case of particles overlapping), increasing then the signal to noise ratio. However, to properly determine the exact movement of the particle between two images, an optical flow (OF) approach is used. OF leads to much better results in terms of precision as typical uncertainties are evaluated at 1/20 of a pixel through detailed experimental validations on well-controlled systems. Furthermore, as a displacement is obtained for each point of the outer ring of the particle, it provides an estimation of the accuracy we can achieve. Finally, the 3D time-resolved signal of the rod displacement at each tracked particle location can be extracted.

3. RESULTS AND DISCUSSION

3.1. 3D flow velocity analysis

The fixed rod configuration is first examined. 3D3C PTV and LDV axial velocity measurements are performed, as aforementioned, in the upstream section at approximately 100 *mm* from the central guide plate, along a line crossing diametrically the rod in the x direction. The resulting 3D3C PTV axial velocity profiles of mean and standard deviation values show a very good agreement with the ones obtained by LDV (see Figure 7). Furthermore, the 3D3C PTV technique appears to be more precise in the near boundary region of the rod (less averaging) along with a level of velocity fluctuation that matches the LDV one both in shape and amplitude. Other aspects of improvements have been observed after upgrading the 3D3C PTV post-processing algorithms. First, the post-processing of the 20 000 frames acquired for this configuration requires 20 hours (instead of 42 hours before optimization on an HP Z820 workstation with 2 Xeon processors of 12 hyper-threaded cores each).

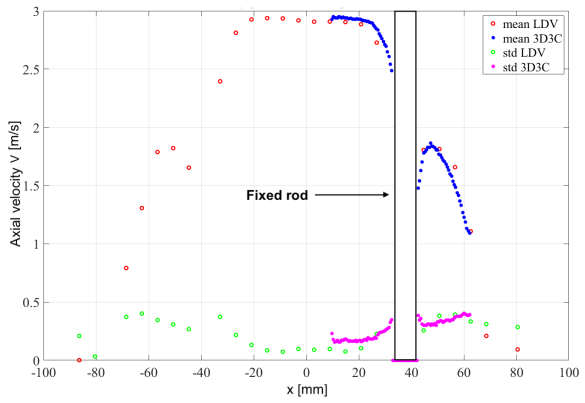

Figure 7. 3D3C PTV and LDV axial velocity V profiles along the line crossing diametrically the fixed rod in the x direction, 100 mm downstream of the guide plate center

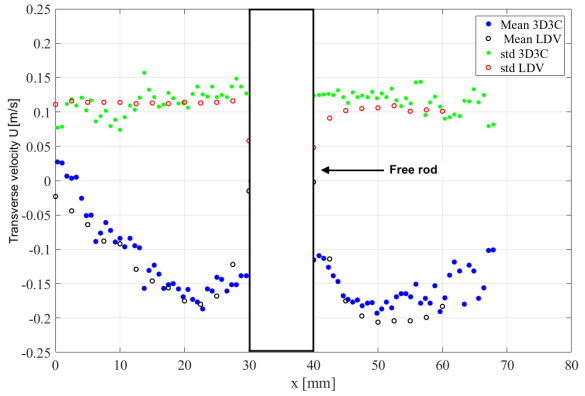

Figure 8. 3D3C PTV and LDV transverse velocity U profiles along the line crossing diametrically the free rod in the x direction

Second, the number of seed particles tracked over three consecutive instants increased by 12%. Such improvement will further enrich the input data for future pressure field reconstruction.

To complete the 3D3C measurements validation on the axial velocity profiles, validation in the transverse direction (x) is proposed to better quantify the measurement uncertainty of this technique for low levels of velocity and fluctuations. Unfortunately, such LDV measurements were not available on the fixed rod configuration, and the experimental setup was modified to accommodate the free and instrumented rod configurations. LDV measurements on the transverse velocity U have then been performed for the free rod configuration. Reader's attention is brought to the fact that in the free and instrumented rod configurations, measurements were operated in the downstream region at approximately 50 *mm* from the central guide plate.

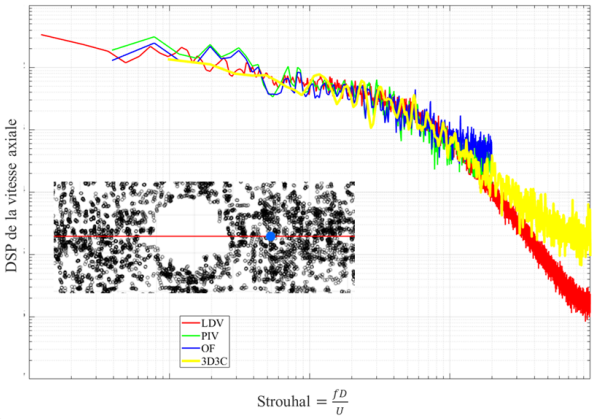

Figure 9. PSD of 3D3C PTV, LDV, PIV and OF axial velocity near the rod downstream of the guide plate

Transverse velocity profiles U, extracted from 3D3C PTV measurements along the line crossing diametrically the free rod in the x direction, demonstrate once again a good agreement with LDV, underlining the accuracy and robustness of the 3D3C PTV technique (see Figure 8) with such low-velocity levels - about 10 times lower than the axial velocities. For time and budget reasons, LDV measurements in the third direction z were not performed for any of these configurations. However, this remaining step is of importance to complete the validation process of the 3D3C PTV technique. We hope that it can be done soon.

After validation of the 3D3C PTV measurements with respect to the spatial distribution, one may focus now on the spectral distribution of the flow in the frame of FIV of the vibrating rods. In the same way, the flow excitation is described by the Power Spectral Density (PSD) of the (axial) velocity. A comparison is made at a point extracted downstream of the guide plate near the fixed rod where recycling flows interact with peripheral jets on the fixed rod configuration. Once again, the agreement with LDV (PIV and OF) is quite good in terms of PSD shape, amplitude and cutoff frequencies (see Figure 9).

3.2. 3D rod displacement analysis

In this section, light is brought on the instrumented rod. For this configuration, particles are fixed at various locations on the rod surface. Whereas seeding particles have a mean convective velocity when following the fluid, the mean displacement of these particles fixed on the rod is null. The displacement of these particles fixed on the rod is expected to be less than 0.5 pixels between two frames. For those particles only, a slightly different tracking approach is taken. Indeed, as the particles are stacked on the rod,

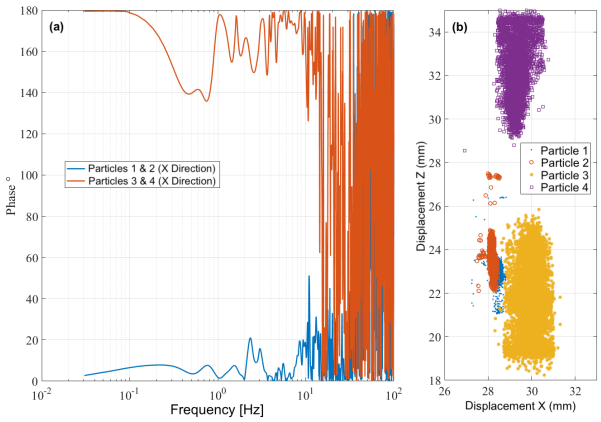

Figure 10. ***(a)*** *Phase between particles 1 & 2 and 3 & 4 displacement signals in the x direction,* ***(b)*** *Four particles, fixed on the instrumented rod surface, movement in the x - z plane*

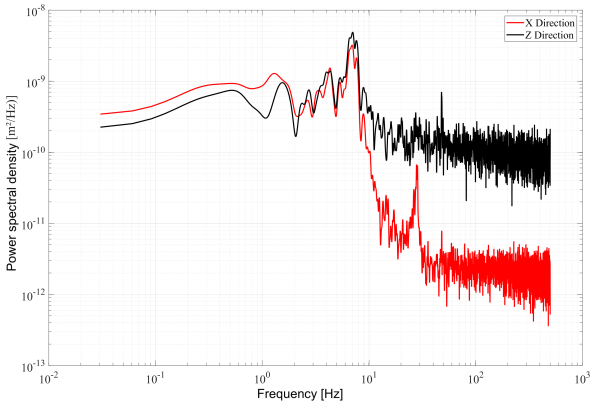

Figure 11. Power spectral density of the x and z particle 1 displacement signals. Instrumented rod case

it is relatively easy to follow them within the entire span of the experiments. Therefore, displacements are not only determined between two consecutive frames but also with respect to the first frame. The average between these two distinct measurements is kept to determine the instantaneous displacements.

Four specific particles are tracked over time. Particles 1 and 2 are located in the top area, while particles 3 and 4 are located further down. However, particles 1, 2 and 3 are located on one side of the rod (in-depth), while particle 4 is on the opposite. The 3D3C improved algorithm was able to track the different particles 1, 2, 3 and 4 over time as forcing a particle to be detected, regardless the quality of the signal. It appears that the tracking efficiency depends on the illumination level of the particle pattern subject to tracking on all acquired frames.

The tracking method allowed identifying the z direction as the main oscillating direction of the flow along which displacements are the most important (see Figure 10). Due to vortex shedding, a rod submitted to a transverse flow oscillates mainly along with its lift (perpendicular to the main flow direction). This seems to support the previous observation on the instrumented rod. A second interesting observation could be made. This rod appears to rotate around itself under the flow. Such a movement is possible due to the fact that the instrumented rod is maintained up and down via strings. This rotating movement was also successfully captured with the tracking method as demonstrated in Figure 10, where one can observe a phase of 180 degrees between particles 3 and 4 displacement signals along the x direction. Meanwhile, no phase is observed between particles 1 and 2 displacement signals along the x direction since both particles belong to the same side (from the camera view). Spectral analysis of the displacement signals, resulting from the tracking process, of the particle 1 along the x and z directions - using Welch's PSD method - also allowed identifying the first vibrating mode around $f = 7\ Hz$ (see Figure 11). Similar results were obtained on the free rod configuration when two particles located at two different positions on its surface were tracked, even if such results are not presented in this paper. We demonstrated in this section the ability of 3D3C PTV based algorithms to capture the FIV of a submerged vibrating structure (rod) finely. Nevertheless, this promising non-intrusive tracking method (with respect to precision) needs to be validated by conventional (intrusive) displacement measurement techniques such as accelerometers, strain gages, and eddy currents sensors.

4. CONCLUSION & PERSPECTIVES

The present study focused primarily on describing 3D3C PTV measurements of the turbulent flow as the excitation source of (control) rods. The technique's ability to capture the flow distribution has been demonstrated from both spatial and spectral perspectives. Post-processing improvements have enabled this thorough validation up to low-velocity levels compared to what has been presented by Fichet et al (2018). Significant gain in computational time was also observed, along with an increase in the number of tracked particles over time. However, even if the in-plane transverse LDV measurements validate the 3D3C PTV measurements, a remaining validation is required along the depth direction (off-plane of the camera image) to fulfil the validation process.

Finally, an innovative non-intrusive technique based on 3D3C PTV enables to access both the fluid velocity (flow excitation) and the structure response (rod displacement) at the same time. How-

ever, this promising technique needs to be further validated by other conventional techniques in order to evaluate its uncertainty levels. Last but not least, pressure field reconstruction will be also carried out around rods, from 3D measured velocity fields, using a pressure gradient integration method inspired by Tronchin (2013). The resulting pressure distribution will be then used to deduce linear forces applied on the rods. Once completed and validated, this 3D3C method would be a very practical tool to study FIV in plenty of test configurations.

5. REFERENCES

Ansari, S. A. et al, 2008, Detection of flow-induced vibration of reactor internals by neutron noise analysis. *IEEE Transactions on Nuclear Science* **55(3)**: 1670–167

Baudoin, R., 2015, Développement d'une technique de vélocimétrie laser en trois dimensions par suivi de particules basée sur le principe de défocalisation et son application autour d'obstacles en aval d'une grille. *PhD, Thesis, Ecole Doctorale n 579 Centrale-Supelec*

Cioncolini, A. et al, 2018, Axial-flow-induced vibration experiments on cantilevered rods for nuclear reactor applications. *Nuclear Engineering and Design* **338**: 102–11

Damaschke, N. et al, 2005, Multidimensional particle sizing techniques. *Experiments in Fluids - EXP FLUID* **39**: 336–3

De Pauw, B. et al, 2013, Benchmarking of deformation and vibration measurement techniques for nuclear fuel pins. *Measurement* **46**: 3647–365

Fichet, V. et al, 2018, PTV 3D3C haute cadence autour d'un cylindre dans une maquette industrielle de carte de guidage. 16^{e} *Congrès Francophone de Techniques Laser pour la Mécanique des Fluides, Dourdan, France* pages: 103–11

Gesemann, S. et al, 2016, From noisy particle tracks to velocity, acceleration and pressure fields using b-splines and penalties. 18^{th} *International Symposium on Applications of Laser Techniques to Fluid Mechanics, Lisbon, Portugal*

Kim, S.-N et al, 2001, The experiment of flow induced vibration in pwr rccas. *KSME International Journal* **15(3)**: 291–2

Moussou, P et al, 2019, Experimental Investigation of the Flow-Induced Vibrations of a Rod Cluster Control Assembly inside Guides with Enlarged Gaps. *2019 Pressure Vessel and Piping Conference* **93143**

Novara, M. et al, 2012, Lagrangian acceleration evaluation for tomographic piv: a particle-tracking based approach. 16^{th} *International Symposium on Applications of Laser Techniques to Fluid Mechanics, Lisbon, Portugal*

Shengjie, G. et al, 2015, Diagnostic techniques for flow induced vibration. 16^{th} *International Topical Meeting on Nuclear Reactor Thermal Hydraulics, Chicago, IL, USA* page 3618

Shono, A. et al, 1985, Control rods vibration analysis in joyo mark-ii core. *Progress in Nuclear Energy* **15**: 293– 301

Tronchin, T., 2013, Caractérisation expérimentale et numérique es mécanismes tourbillonnaires de génération de portance sur une aile en mouvement couplé de battement et tangage. *PhD Thesis, ISAE, Poitiers*